

SANDIA REPORT

SAND87-1689 • UC-60
Unlimited Release
Printed January 1988

RS-8232-2/66619

cy 1

Analysis of Wind Turbines on Offshore Support Structures Excited by Random Wind and Random Waves



8232-2//066619



00000001 -

Debby S. Oscar, Thomas L. Paez

Prepared by
Sandia National Laboratories
Albuquerque, New Mexico 87185 and Livermore, California 94550
for the United States Department of Energy
under Contract DE-AC04-76DP00789



1139967

Issued by Sandia National Laboratories, operated for the United States Department of Energy by Sandia Corporation.

NOTICE: This report was prepared as an account of work sponsored by an agency of the United States Government. Neither the United States Government nor any agency thereof, nor any of their employees, nor any of their contractors, subcontractors, or their employees, makes any warranty, express or implied, or assumes any legal liability or responsibility for the accuracy, completeness, or usefulness of any information, apparatus, product, or process disclosed, or represents that its use would not infringe privately owned rights. Reference herein to any specific commercial product, process, or service by trade name, trademark, manufacturer, or otherwise, does not necessarily constitute or imply its endorsement, recommendation, or favoring by the United States Government, any agency thereof or any of their contractors or subcontractors. The views and opinions expressed herein do not necessarily state or reflect those of the United States Government, any agency thereof or any of their contractors or subcontractors.

Printed in the United States of America
Available from
National Technical Information Service
U.S. Department of Commerce
5285 Port Royal Road
Springfield, VA 22161

NTIS price codes
Printed copy: A02
Microfiche copy: A01

Distribution
Category UC-60

SAND87-1689
Unlimited Release
Printed January 1988

Analysis of Wind Turbines on Offshore Support Structures

Excited by Random Wind and Random Waves

Debby S. Oscar, Thomas L. Paez
Wind Energy Research Division
Sandia National Laboratories
Albuquerque, NM 87185

ABSTRACT

A numerical approach has been developed to predict the dynamic response of structures excited by random wind and random waves, such as wind turbines at offshore locations. The software developed by this effort, called OFFSHORE HAWTDYN, calculates the displacement time response of horizontal axis wind turbines (HAWTs) attached to offshore support structures subjected to steady and random wind and wave forces that simulate ocean environments. This software utilizes the structural dynamic analysis capability of HAWTDYN, a code developed at Sandia National Laboratories, to solve the equations of motion. The HAWTDYN code was modified to permit the application of water wave loads to the structure being analyzed.

INTRODUCTION

The concept of placing wind turbines on ocean-based platforms is motivated by a desire to use the large offshore wind energy resource of relatively shallow waters, as well as to alleviate the environmental impact of land-based turbines. A wind turbine in an ocean environment will be loaded by turbulent and steady wind on the rotor and wave forces on the support structure. The software package, OFFSHORE HAWTDYN (OFFSHORE Horizontal Axis Wind Turbine Dynamics), is the result of incorporating all of these load cases into a structural dynamics model of an ocean-based horizontal axis wind turbine, with particular interest in developing an analytical model of the wave loads. The result is the calculation of structural dynamic response of the turbine and support structure as displacement time histories. The power spectral densities (PSD) and root mean square responses are also calculated. The structural response is calculated by HAWTDYN, a structural code developed by Lobitz.¹ The aerodynamic loads on the rotor are computed by the Prop Code.² These loads are the result of mean axial wind, turbulence, and aeroelastic effects. A spatially coherent model of the wind turbulence was developed by Veers.³ The efficient design and construction of wind turbines placed on offshore support structures excited by environmental loads depend on the availability of tools to make a structural dynamic analysis.

The basic tool for analysis, developed at Sandia National Laboratories (SNL), is a structural dynamics code for land-based horizontal axis wind turbines subjected to wind loading. This code, HAWTDYN, has been augmented to incorporate a finite element model of an offshore support structure loaded by random waves. The mass, stiffness, and damping matrices of the stationary tower and support structure and of the rotating rotor are produced by NASTRAN (a linear code) and utilized by HAWTDYN. The support structure and tower are modeled in a fixed reference frame, and the rotor is modeled in a rotating reference frame at a constant angular velocity. HAWTDYN was selected for the structural dynamic analysis based on its success in predicting mean and cyclic flapwise bending moment for the rotor of the 2.5 MW MOD2 HAWT.¹ In addition, HAWTDYN predicts natural frequencies of the MOD2 and qualitatively predicts teeter response behavior to

wind shear. The addition of a finite element model of a stationary support structure loaded by random waves extends the HAWTDYN capability as a design tool for the general problem of stochastically loaded offshore structures that have a rotating substructure attached to a fixed foundation.

A turbulent wind field is generated by Veers' code,³ which uses a power spectral density and coherence of the wind provided by Frost, Long, and Turner.⁴ Turbulent wind velocity is modeled as a function of wind speed, height above ground, and surface roughness coefficient. The spatial correlation of the wind is specified by a coherence function. Steady and turbulent wind velocities are used to establish loads on the rotor using the PROP code, which uses momentum theory aerodynamics.

Random wave loads are established as a function of water particle velocity and acceleration. Water particle velocities and accelerations are obtained by summing functions of wave height amplitude over a range of frequencies. To generate a time history of wave height amplitude, many harmonic components are summed with random phase. The water particle velocities and accelerations are perfectly coherent so that each time history in space is deterministically related to every other time history by linear wave theory. Assumptions associated with linear wave theory are that flow is undisturbed by the structure and that wave height is small compared to water depth and wave length. The mean square frequency content of wave height is represented by a PSD. The underlying spectral content is represented by either the Pierson-Moskowitz PSD⁵ for fully developed seas or the Fetch-Limited (JONSWAP) PSD⁶ for underdeveloped sea states.

Water particle velocities and accelerations must be generated at Gauss points along the length of every submerged structural member to allow for integration of point forces into total force. A two-point per element Gaussian integration scheme was chosen. In this analysis, waves can impinge on any arbitrarily oriented structural member from any direction. The component of water particle velocity and acceleration perpendicular to the member is determined. These velocities and accelerations are incorporated in the wave load expression, known as

Morison's equation. Loads generated perpendicular to the member are integrated, and loads parallel to the member's length are neglected. The fundamental measure of structural dynamic response is the displacement time history of the composite turbine and support structure. This graphical representation of the motion of the structure is computed in the augmented HAWTDYN code, called OFFSHORE HAWTDYN. Other measures of structural response, including power spectral density and root mean square responses, are also calculated.

OCEAN WAVE LOAD EQUATIONS

The fluid-induced loads on submerged structures are obtained from a gravity wave model. Linear wave theory is used as the basis for a probabilistic spectral description of the waves. An indepth discussion of linear wave theory can be found in the ocean engineering text by Wilson.⁷ There are nine assumptions inherent in linear wave theory.

1. The amplitude, A, of the surface disturbance (wave height) is very small relative to the wave length, λ , and depth, d.
2. The velocity head $(u + w)/2g$ is negligible compared with the anomaly of pressure head (from hydrostatic conditions), where u and w are the horizontal and vertical particle velocities, respectively.
3. The fluid has a uniform depth, d.
4. The fluid is nonviscous and irrotational.
5. The fluid is incompressible and nonstratified (homogeneous).
6. The deflecting force associated with the earth's rotation (Coriolis force) is negligible.
7. Surface tension is negligible.
8. The bottom is smooth and impermeable.
9. The sea level atmospheric pressure, p_a , is uniform. The water pressure is denoted by p.

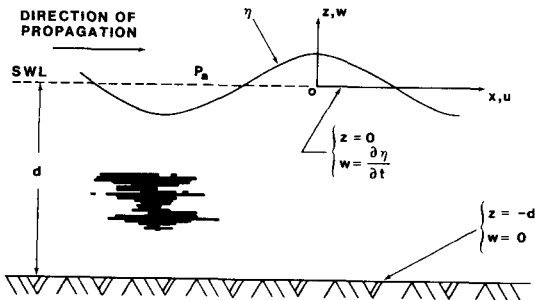


Figure 1. Schematic representation of a simple harmonic wave.

The linear model for surface gravity waves yields a sinusoidal surface profile, which propagates with constant velocity. The surface profile takes on the form

$$\eta(x,t) = A \cos(kx - \omega t), \quad (1)$$

where

- A = wave amplitude
- k = wave number
- ω = natural frequency (radians/second).

Linear wave theory provides a functional relationship between wave heights and water particle velocities and accelerations in space over time. When used to describe a spatial wave field over time, this relation characterizes the water particle velocities and accelerations as perfectly coherent. Expressions 2 through 5 for water particle velocities and accelerations can be viewed as harmonic functions multiplied by functional forms that depend on frequency, ω , depth below the water surface of a point of interest, z, and absolute water depth, d. In order to form realizations of wave height random processes, particle velocity random processes, etc., these harmonic components from Equations (1) through (5) are added together over all frequencies. The amplitude at each specific frequency is chosen so that the wave height random process has a specified PSD. The random process realizations have zero mean.

$$\text{Horizontal particle velocity} \\ u = A \omega \frac{\cosh k(z+d)}{\sinh(kd)} \cos(kx - \omega t) \quad (2)$$

$$\text{Vertical particle velocity} \\ w = A \omega \frac{\sinh k(z+d)}{\sinh(kd)} \sin(kx - \omega t) \quad (3)$$

$$\text{Horizontal particle acceleration} \\ \dot{u} = \frac{4 \pi^2 A}{T^2} \frac{\cosh k(z+d)}{\sinh(kd)} \sin(kx - \omega t) \quad (4)$$

$$\text{Vertical particle acceleration} \\ \dot{w} = \frac{-4 \pi^2 A}{T^2} \frac{\sinh k(z+d)}{\sinh(kd)} \cos(kx - \omega t) \quad (5)$$

where $T = 2\pi/\omega$ is the period of a particular harmonic component. Wave number k is related to the natural frequency as defined by a transcendental equation:

$$\omega^2 = gk \tanh(kd). \quad (6)$$

This relation indicates that the frequency of each harmonic determines the velocity at which it will propagate in space and that each frequency propagates at a different rate. Since wave number is a function of frequency, its value must be uniquely determined for each harmonic component of the signal.

The generation of a random process realization is accomplished in the following way. Based on the discrete form of Fourier series representation for periodic signals, a random time series, x_j , is represented as a summation of many harmonic components with random phase:

$$x_j = \sum_{k=0}^{N-1} X_k e^{i(2\pi jk/N - \phi_k)}, \text{ for } j = 0, 1, \dots, N-1 \quad (7)$$

where ϕ_k = randomly generated phase.

To create real-valued, random time histories with zero mean, it is necessary to impose the following conditions:

1. X_k is real-valued for $k = 1, 2, \dots, (N/2)-1$
2. $X_0 = X_{N/2} = 0$
3. $X_{(N/2)+k} = X_{(N/2)-k}$ for $k = 1, 2, \dots, (N/2)-1$
4. $\phi_k = \text{uniform} [-\pi, \pi]$, $k = 1, 2, \dots, (N/2)-1$
5. $\phi_{(N/2)+k} = -\phi_{(N/2)-k}$ for $k = 1, 2, \dots, (N/2)-1$.

With these conditions imposed on Equation (7), it can be transformed to become:

$$x_j = 2 \sum_{k=0}^{N/2} X_k \cos(2\pi jk/N - \phi_k), \quad j = 0, 1, 2, \dots, N-1. \quad (8)$$

With the appropriate definition of X_k , this representation will produce a real, zero mean, random time signal with any desired spectral density. The form of Equation (8), representing a randomly generated time history as a summation of terms that are amplitudes multiplied by harmonic functions makes Equation (8) a compatible representation for modeling Equations (1) through (5). The x_j represents randomly generated wave height amplitudes, $\eta(0, t)$. Equation (7) is the inverse Fourier transform of $X_k e^{-i\phi_k}$. A fast Fourier transform algorithm is used to execute the discrete Fourier transform of Equation (7).

The random phases in Equation (7), ϕ_k , are the quantities that randomize the signal x_j , for $j = 0, 1, \dots, N-1$. The ϕ_k is generated as a uniform random variable on the interval $[-\pi, \pi]$. Each ϕ_k is independent of ϕ_m for $k \neq m$. The values of the X_k , $k = 0, 1, \dots, N-1$, establish the spectral density of the random signal. When the series X_k , $k=0, \dots, N-1$ are chosen using the formula, $X_k = [\Delta\omega S_{XX}(\omega)]^{1/2}$, the realization of the random process formed using Equation (7) has the underlying spectral density $S_{XX}(\omega)$. $S_{XX}(\omega)$ is assumed to be a two-sided spectral density. For a one-sided PSD, $G_{XX}(\omega)$, $X_m = [1/2 \Delta\omega G_{XX}(\omega)]^{1/2}$.

The two PSDs used to describe the frequency content of wave amplitudes observed in the sea are

- 1) Pierson-Moskowitz spectrum for fully developed sea conditions
 - 2) Fetch-Limited (JONSWAP) spectrum.
- The Pierson-Moskowitz PSD is given by Equation (9).

$$S_{XX}(\omega) = \frac{8.1 \times 10^{-3}}{\omega^5} g^2 e^{-0.74(g/V\omega)^4}, \quad \text{where} \quad (9)$$

V = windspeed at a height of 19.5 meters above still water level
 ω = natural frequency (radians/sec).

An example of the Pierson-Moskowitz PSD for a 27-mph mean wind is shown in Figure 2.

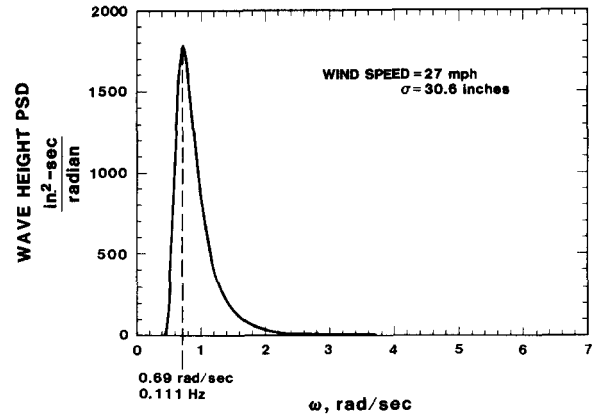


Figure 2. Pierson-Moskowitz PSD.

Fully developed sea states are characterized by power content at low frequencies and high wave heights. The Fetch-Limited PSD for less exposed areas is given by Equation (10).

$$S_{XX}(\omega) = \alpha^2 \omega^{-5} \exp[-B(\frac{\omega}{\omega_m})^{-4}] \zeta \exp[-(\omega - \omega_m)^2 / 2\sigma^2 \omega_m^2] \quad (10)$$

where $B = 1.25$
 $\zeta = \begin{cases} 7.0 & \text{for very peaked spectra} \\ 3.3 & \text{for mean of selected JONSWAP data} \\ 1.0 & \text{Pierson-Moskowitz spectrum} \end{cases}$
 $\sigma = \begin{cases} 0.07 & \text{for } \omega \leq \omega_m \\ 0.09 & \text{for } \omega > \omega_m \end{cases}$

$$\omega_m = \text{peak frequency} = 2\pi(3.5)(g/V)(\bar{X})^{-0.33}$$

$$\alpha = 0.076(\bar{X})^{-0.22}$$

$\bar{X} = gX/V^2$
 X = fetch length
 V = wind speed.

The Fetch-Limited spectrum requires three environmental input parameters:

- 1) Fetch length, X
- 2) Windspeed at 10 meters above still water level, V
- 3) A shape parameter, ζ , defined as the ratio of the maximum spectral energy at peak frequency to the spectral energy of the corresponding Pierson-Moskowitz spectrum.

An example of the Fetch-Limited PSD for a 27-mph mean wind is shown in Figure 3.

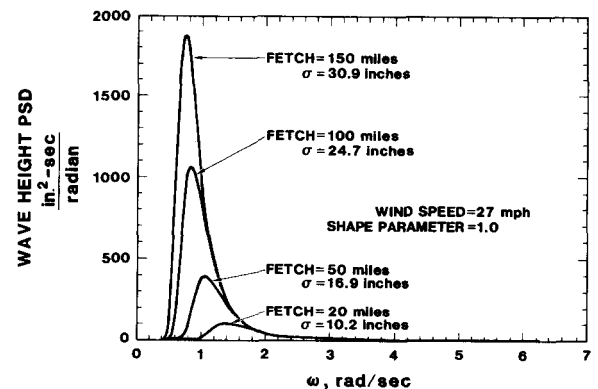


Figure 3. Fetch-Limited (JONSWAP) PSD.

The wave height spectrum for less exposed areas produces power at higher frequencies and lower amplitudes than the fully developed spectrum. Waves can approach an arbitrarily oriented structural member from any possible direction. Waves are planar and can be applied from any angular direction between 0° and 360°. Time histories of wave particle velocities and accelerations must be randomly generated at the points in space that represent the Gauss points of each finite element to prepare for the integration of distributed forces into total load. Water particle velocities and accelerations are randomly generated at the two Gauss points along the length of each submerged finite element.

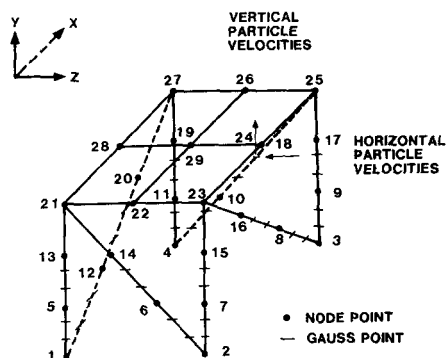
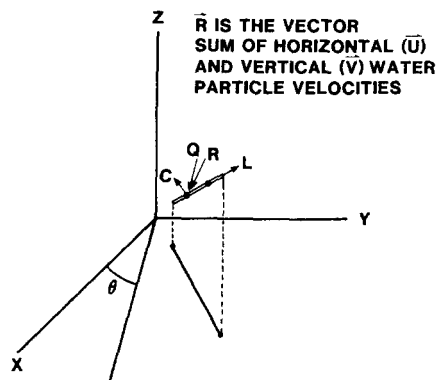


Figure 4. Finite element nodal and Gauss points along length of member using two point Gaussian quadrature.

The components of water particle velocity and acceleration perpendicular and parallel to the member must be determined to decompose the loads into the local elemental coordinate system. The component of the load perpendicular to the structural member is applied, and the component of the load parallel to the member is neglected. To find water particle velocity perpendicular to the member, first the vector sum of horizontal and vertical water particle velocities is found; denote it \vec{R} : ($\vec{R} = U \cos\theta \hat{i} + U \sin\theta \hat{j} + V \hat{k}$). A cross product is formed between the velocity vector and a vector occurring along the length of the structural member, \vec{L} . This creates a third vector, $\vec{C} = \vec{R} \times \vec{L}$, that is perpendicular both to the original velocity vector and the member. Then a cross product is taken between the member vector \vec{L} and \vec{C} to create a vector, $\vec{Q} = \vec{L} \times \vec{C}$. The vector \vec{Q} is perpendicular to the member and lies in the original plane created by the member and the original velocity vector. \vec{Q} vector represents the direction of interest. A unit vector, \vec{Q}_{unit} , in the direction of \vec{Q} is formed ($\vec{Q}_{unit} = \vec{Q}/|\vec{Q}|$). Finally, a dot product between \vec{Q}_{unit} and the original velocity vector, \vec{R} , is taken to establish the component of \vec{R} perpendicular to the member, \vec{S} ($\vec{S} = \vec{Q}_{unit} \cdot \vec{R}$). The same procedure is applied to water particle accelerations.



θ = WAVE DIRECTION
 $\vec{R} = U (\cos\theta)\hat{i} + U (\sin\theta)\hat{j} + V \hat{k}$ = VELOCITY VECTOR
 FIND $\vec{C} = \vec{R} \times \vec{L}$ -- A VECTOR PERPENDICULAR TO VELOCITY VECTOR AND MEMBER.
 FIND $\vec{Q} = \vec{L} \times \vec{C}$ -- A VECTOR PERPENDICULAR TO MEMBER IN THE PLANE CREATED BY MEMBER AND VELOCITY VECTOR.
 $\vec{Q}_{UNIT} = \frac{\vec{Q}}{|\vec{Q}|}$ -- UNITIZE \vec{Q} TO RETAIN ITS DIRECTION.
 FIND $\vec{S} = \vec{Q}_{UNIT} \cdot \vec{R}$ -- ACHIEVE COMPONENT OF VELOCITY VECTOR PERPENDICULAR TO MEMBER.

Figure 5. Component of water particle velocity perpendicular to member.

The velocities and accelerations perpendicular to the member are incorporated in the wave force expression known as Morison's equation. Morison's equation is the vector sum of a drag term due to water particle velocities and an inertia term due to water particle accelerations. The full expression for Morison's equation that results in force per unit length is Equation (11).

$$F_{\alpha} = 1/2 C_D \rho D U_{\alpha}^2 + C_M \rho \pi (D^2/4) \dot{U}_{\alpha}, \quad (11)$$

where

- α = x, y, z, directions
- C_D = drag coefficient (1.0 was used)
- C_M = inertia coefficient (1.5 was used)
- ρ = density of sea water
- D = diameter
- U_{α} = flow velocity
- \dot{U}_{α} = flow acceleration.

Point load time histories are integrated over the length of the structural member and redistributed to the nodal endpoints with the concept of virtual work and the approximation that the structural deformation varies linearly between endpoints. A virtual work approach is used to show that an incremental amount of work is equal to an incremental deflection times the applied force;

$$\delta \bar{W}(s) = \delta \bar{u}(s)^T \cdot \bar{F}(s).$$

A linear interpolation of translational deformation between the endpoints of a structural member is found with the following relation:

$$\delta \bar{u}(s) = \begin{bmatrix} 1-s & 0 & 0 & s & 0 & 0 \\ 0 & 1-s & 0 & 0 & s & 0 \\ 0 & 0 & 1-s & 0 & 0 & s \end{bmatrix} \begin{bmatrix} \delta u_{x_1} \\ \delta u_{y_1} \\ \delta u_{z_1} \\ \delta u_{x_2} \\ \delta u_{y_2} \\ \delta u_{z_2} \end{bmatrix}$$

$$\delta \bar{u}(s) = [S] \cdot \delta \bar{u}$$

The distributed virtual work follows:

$$\delta \bar{W}(s) = \delta \bar{u}^T \begin{bmatrix} 1-s & 0 & 0 \\ 0 & 1-s & 0 \\ 0 & 0 & 1-s \\ s & 0 & 0 \\ 0 & s & 0 \\ 0 & 0 & s \end{bmatrix} \begin{bmatrix} F_x(s) \\ F_y(s) \\ F_z(s) \end{bmatrix}$$

Integrate over the length of the beam, L:

$$\delta \bar{W} = \delta \bar{u}^T L \int_0^1 \begin{bmatrix} 1-s \\ 1-s \\ 1-s \\ s \\ s \\ s \end{bmatrix} \begin{bmatrix} F_x(s) \\ F_y(s) \\ F_z(s) \\ F_x(s) \\ F_y(s) \\ F_z(s) \end{bmatrix} ds$$

A two-point Gaussian quadrature is used to evaluate the integrals:

$$\begin{bmatrix} F_{x_1} \\ F_{y_1} \\ F_{z_1} \\ F_{x_2} \\ F_{y_2} \\ F_{z_2} \end{bmatrix} = L \int_0^1 \begin{bmatrix} 1-s \\ 1-s \\ 1-s \\ s \\ s \\ s \end{bmatrix} \begin{bmatrix} F_x(s) \\ F_y(s) \\ F_z(s) \\ F_x(s) \\ F_y(s) \\ F_z(s) \end{bmatrix} ds$$

WIND LOADS AND ANALYSIS OF WIND TURBINES

The wind velocities used in aerodynamic load calculations include the mean axial wind, aeroelastic effects due to local velocity and twisting deformation of the blade, and stochastic wind turbulence. The mean axial wind velocities are predicted by the PROP code, which uses momentum theory to compute interference factors, ϵ . The relative wind velocity vector is given by the following expression:

$$W_r = (1 - \epsilon)W_m + W_{si} - [\dot{U}_R + \Omega \times (X_R + U_R)] \quad (12)$$

where W_m is the mean axial wind
 W_{si} is the stochastic wind
 Ω is the rotational velocity of the turbine
 X_R is the initial local position vector
 U_R is blade deformation
 \dot{U}_R is the velocity of blade flexibility.

With the relative wind velocity vector determined, aerodynamic loads applied to the rotor are determined through lift and drag formulations. The lift (L) and drag (D) forces per unit length are given by

$$L = 1/2 \rho a W_N^2 C_L(\alpha)$$

$$D = 1/2 \rho a W_N^2 C_D(\alpha),$$

where ρ = density of air
 a = length of chord
 C_L, C_D = coefficients of lift and drag
 α = angle of attack
 W_N = chordwise direction of wind velocity.

The power spectral density of atmospheric turbulence is

$$12.3 V h [\ln(10/z_0 + 1) \ln(h/z_0 + 1)]^{-1}$$

$$S(f) = \frac{12.3 V h [\ln(10/z_0 + 1) \ln(h/z_0 + 1)]^{-1}}{1 + 192.0 [h f \ln(10/z_0 + 1)/V \ln(h/z_0 + 1)]^{5/3}}$$

where
 f = frequency (Hertz) (14)
 h = height above ground
 V = mean speed at $h = 10$ meters
 z_0 = surface roughness coefficient

A surface roughness coefficient of 0.25 was used representing a turbulent wind site. This may be higher than is necessary to model an ocean environment. An example of an atmospheric turbulence PSD is shown in Figure 6.

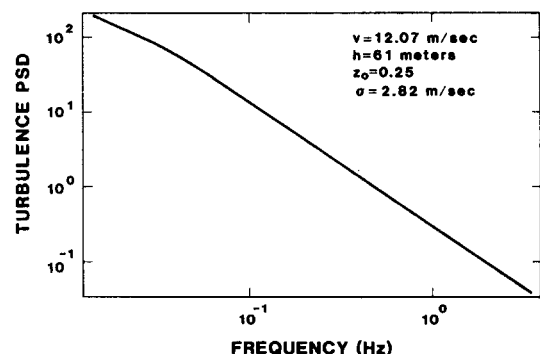


Figure 6. PSD of atmospheric turbulence.

The spatial coherence is $\gamma_{ij}^2 = \exp(-a \cdot \omega \cdot \Delta r / V)$, (15)

where a = decay coefficient = (7.5 was used)
 ω = frequency (Hertz)
 Δr = distance between points i and j
 (meters)
 V = mean windspeed (meters/sec).

The level of correlation depends on the distance between the points, the mean windspeed, and frequency. This coherence function is shown in Figure 7.

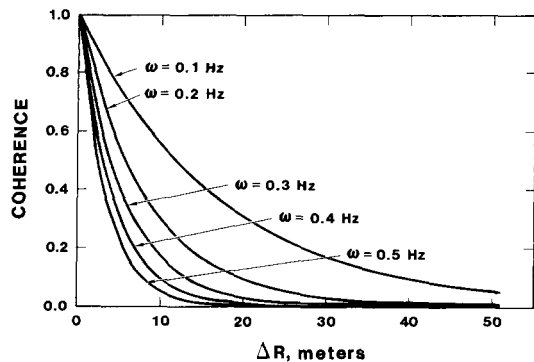


Figure 7. Coherence function, γ^2 , for atmospheric turbulence at a 27-mph mean windspeed.

A schematic of a wind simulation with variations in three dimensions is shown in Figure 8.

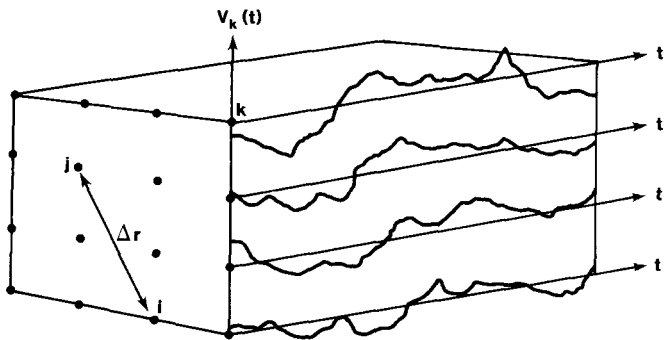


Figure 8. Three-dimensional, spatially varying turbulence.

Correlated single-point time series are generated at several points. It is visually apparent that the lower frequencies in the wind are highly correlated, and the higher frequencies retain less correlation. Turbulent wind random processes with predetermined spectral content and coherence are created as a linear function of uncorrelated, independent random processes. See Veers³ for an example of this calculation.

An example of creating two random processes is shown to illustrate the procedure. Let $X_1(t)$ and $X_2(t)$ be uncorrelated, zero mean, random processes. Let $Y_1(t) = a_{11}(\omega) \cdot X_1(t)$ and $Y_2(t) = a_{21}(\omega) \cdot X_1 + a_{22}(\omega) \cdot X_2(t)$. In matrix form:

$$\begin{bmatrix} Y_1(t) \\ Y_2(t) \end{bmatrix} = \begin{bmatrix} a_{11}(\omega) & 0 \\ a_{21}(\omega) & a_{22}(\omega) \end{bmatrix} \begin{bmatrix} X_1(t) \\ X_2(t) \end{bmatrix}$$

The autocovariance of the vector of random processes of $Y(t)$ is

$$\begin{aligned} R_{YY}(\tau) &= E \{ [Y(t)] [Y(t+\tau)]^T \} \\ &= E \{ [A] [X(t)] [X(t+\tau)]^T [A]^T \} \\ &= [A] R_{XX}(\tau) [A]^T, \end{aligned}$$

where $R_{XX}(\tau) = E \{ [X(t)] [X(t+\tau)]^T \}$.

The power spectral density is the Fourier transform of the autocovariance:

$$\begin{aligned} S_{YY}(\omega) &= \frac{1}{2\pi} \int_{-\infty}^{\infty} R_{YY}(\tau) e^{-i\omega\tau} d\tau \\ &= \begin{bmatrix} S_{Y_1Y_1}(\omega) & S_{Y_1Y_2}(\omega) \\ S_{Y_2Y_1}(\omega) & S_{Y_2Y_2}(\omega) \end{bmatrix} = [A] S_{XX}(\omega) [A]^T. \end{aligned}$$

Since $X_1(t)$ and $X_2(t)$ are uncorrelated white noise random processes, the spectral density matrix between the random processes $[X(t)]$ can be chosen to be the identity matrix. The cross correlation of white noise is zero creating a zero cross spectral distribution, and the spectral density of white noise is chosen to have a magnitude of unity over all frequencies:

$$S_{XX}(\omega) = \begin{bmatrix} S_{X_1X_1}(\omega) & S_{X_1X_2}(\omega) \\ S_{X_2X_1}(\omega) & S_{X_2X_2}(\omega) \end{bmatrix} = \begin{bmatrix} 1 & 0 \\ 0 & 1 \end{bmatrix}$$

Therefore, $S_{YY}(\omega) = [A][A]^T$.

The coherence between $[Y_1(t)]$ and $[Y_2(t)]$ is represented as $\gamma(\omega)$, where

$$\gamma^2(\omega) = \frac{S_{Y_1Y_2}(\omega)^2}{S_{Y_1}(\omega) S_{Y_2}(\omega)}$$

AUGMENTATION OF HAWTDYN

Lobitz¹ developed a computer code, HAWTDYN, for structural dynamic analysis of horizontal axis wind turbines. It uses the finite element code MSC/NASTRAN to generate mass, stiffness, and damping matrices of the tower and rotor, which are treated in NASTRAN as separate structures. The rotor is subsequently joined to the tower externally to NASTRAN, using a time-dependent transformation consistent with the hub configuration. These time-dependent constraint equations account for rotor-tower interactions by allowing for relative motion between the rotor and hub. Rotating frame effects are taken into account by modifying the rotor stiffness matrix due to centrifugal stiffening. Coriolis forces result in the modification of the stiffness and damping matrices. The aerodynamic loads are applied to the turbine blades and the equations of motion are solved in the time domain by the Newmark-Beta method using the time step of 0.008 seconds. The equations of motion are

$$M_T \ddot{U} + C_T \dot{U} + K_T U = F_T + F_W \quad \text{TOWER AND SUPPORT}$$

$$M_R \ddot{U}_R + (C_R + C_\Omega) \dot{U}_R + (K_R - S_\Omega) U_R = F_C + F_G + F_A \quad \text{ROTOR,}$$

- where subscript T = tower and support structure
 subscript R = rotor (16)
 C_Ω = Coriolis matrix
 S_Ω = softening matrix
 F_W = wave forces
 F_C = centrifugal forces
 F_G = gravitational forces
 F_A = aerodynamic forces
 U = displacement vector
 \dot{U} = velocity vector
 \ddot{U} = acceleration vector.

The MOD2 HAWT was modeled in HAWTDYN as an initial test of the code's performance. The MOD2 HAWT has a 300 foot diameter rotor rated at 2.5 MW and was tested in Goodnoe Hills, WA. The finite element model of the MOD2 HAWT used in HAWTDYN is shown in Figure 9.

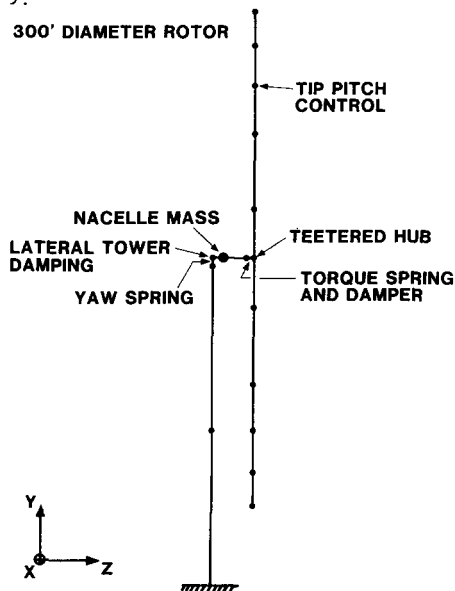


Figure 9. Finite element model of MOD2 HAWT.

OFFSHORE HAWTDYN expands HAWTDYN capabilities to include a finite element model of an offshore support structure loaded by random waves. A code has been developed that generates perfectly coherent, quasi-stationary, random time histories of wave particle velocities and accelerations in three-dimensional space, which are transformed into force-per-unit length. These forces are applied to the support structure at nodal points located below the still water level. A revised finite element model of the turbine and platform structure is shown in Figure 10. The nodal points and Gauss points using two-point Gaussian quadrature are also shown.

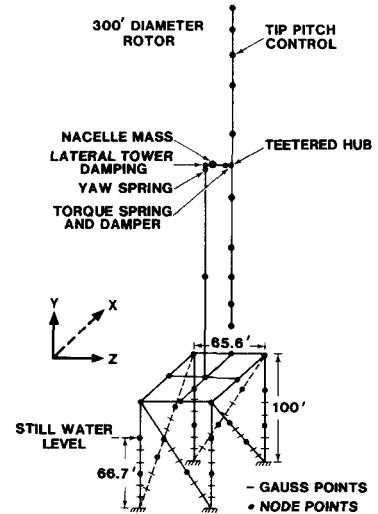


Figure 10. Revised composite finite element turbine/platform structure.

EXAMPLE PROBLEM

An example problem is presented for three separate load conditions. The response to each load condition is shown at different points on the structure. The first set of loads on the structure is steady and turbulent wind at a mean wind of 27 mph, with no wave forces applied. This represents the original capability of HAWTDYN, except that the support structure has been added. A second set of loads represents the isolation of the effect of wave forces on the structure, although the turbine is rotating at 17.5 rpm. For this loading case, the density of air was set to zero, which can be interpreted as rotation of the rotor in a vacuum. The third set of loads involves the fully loaded structure with 27-mph turbulent and steady winds and random waves generated by a 27-mph wind. The Pierson-Moskowitz PSD was used for the underlying spectral content of the wave loads. Horizontal and vertical water particle velocities and accelerations are generated at every Gauss point. A representative picture of horizontal water particle velocity is shown in Figure 11.

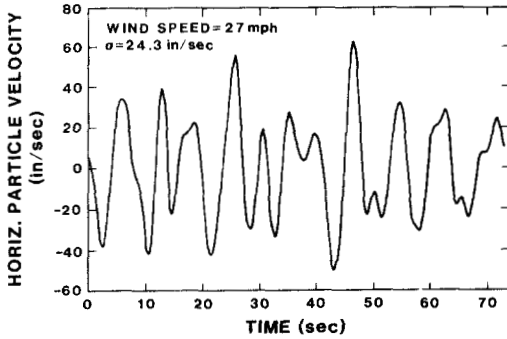


Figure 11. Horizontal water particle velocity.

The code is capable of handling mean horizontal water particle velocities due to tidal current and wind-stress current. A mean horizontal velocity can be superimposed on the randomly generated signal. Tidal current is represented as a power law.

$$U_t(z) = (1 + z/d)^{1/7} U_t(0)$$

where d is the water depth, z is measured positive upward (or negative downward) from the sea surface, and $U_t(0)$ is the surface velocity at $z = 0$.

The other important current is that due to sustained wind blowing over the sea surface. The velocity profile of this wind-stress current is approximated as linear, with a maximum value $U_w(0)$ at the sea surface. The wind-stress current $U_w(z)$ is given by

$$U_w(z) = (1 + z/d) U_w(0)$$

Figure 12 shows a sample of randomly generated wave heights which is a realization of a stationary random process with the underlying Pierson-Moskowitz spectral content for a steady 27-mph wind.

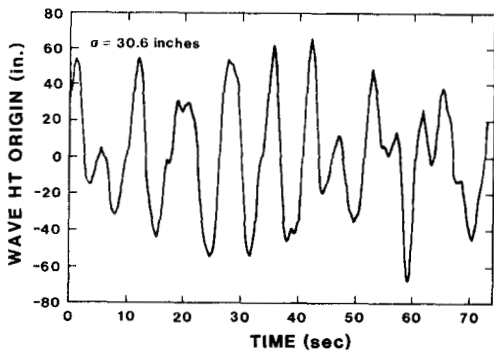


Figure 12. Randomly generated wave heights.

Loads are integrated over the length of the finite element and redistributed to the nodal endpoints in units of force. An example of the integrated wave force in the $-Z$ direction is shown in Figure 13.

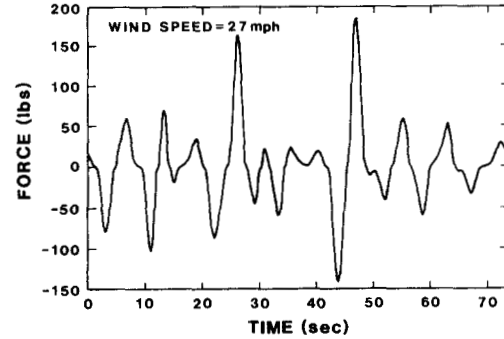
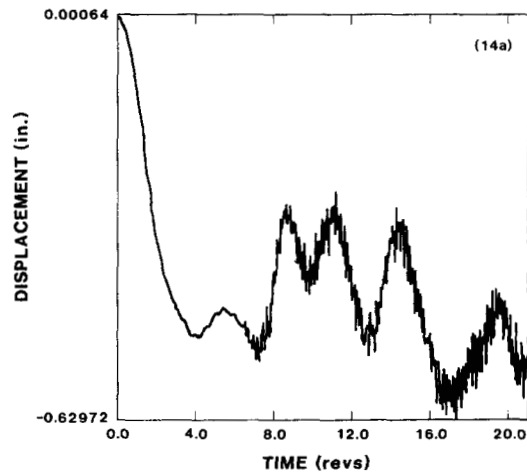


Figure 13. Integrated force at a nodal point in $-Z$ direction.

Displacement structural response for the turbine and support structure is shown at three locations:

1. Center of the platform, Z-direction
2. Top of the turbine tower, Z-direction
3. Center of the platform, Y-direction.

The Z-direction is the orientation of the strongest components of wind forces. Displacement response in units of inches is shown for three different loading cases. The term "wind alone" refers to displacement response due to steady and turbulent winds, with no wave forces applied. The turbine is rotating at 17.5 rpm. The term "waves alone" refers to the loading case of stochastic waves generated by a 27-mph wind. Although the turbine is rotating at 17.5 rpm, no loads are generated by wind. The term "wind and waves" refers to the full loading case of 27-mph turbulent and steady wind on a rotating turbine and random waves on the submerged support structure.



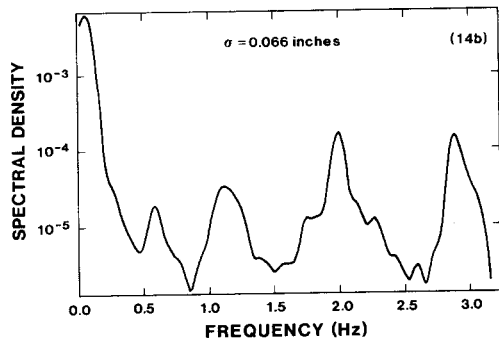


Figure 14. (a) Displacement response of center of platform in Z-direction due to wind loads only.
 (b) PSD of response.

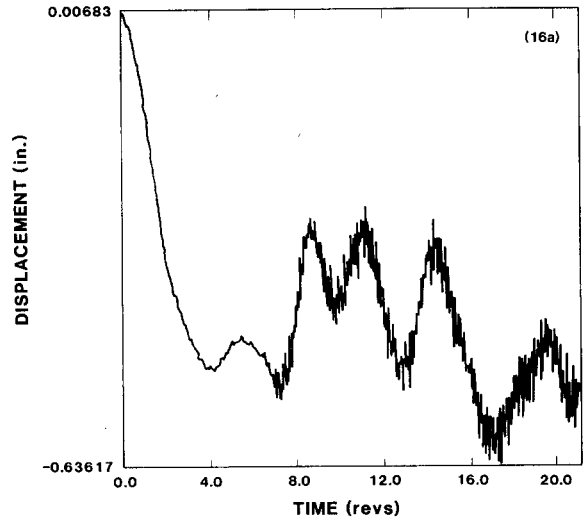


Figure 16. (a) Displacement response of center of platform in Z-direction due to wind and wave loads.
 (b) PSD of response.

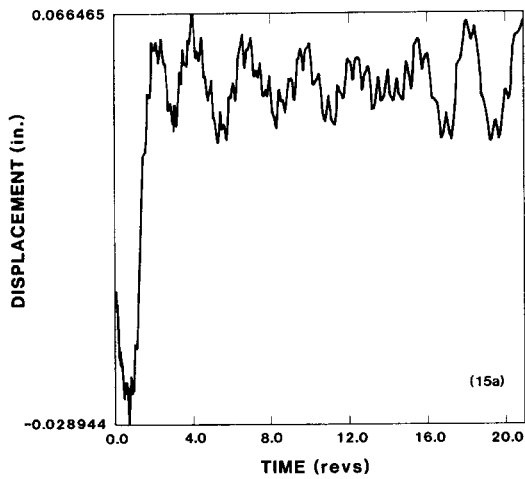
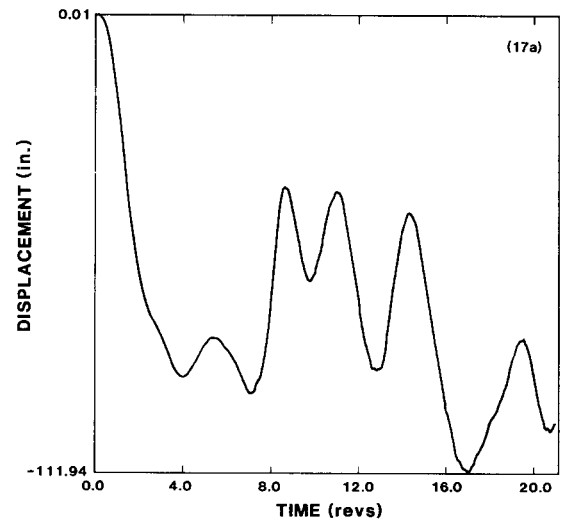
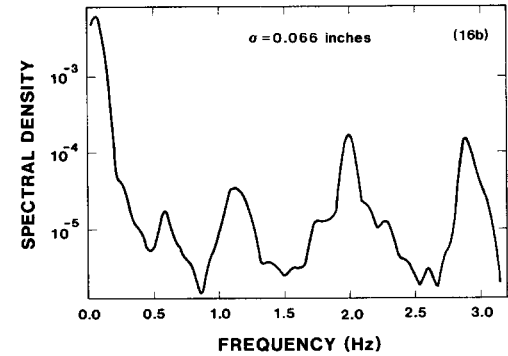
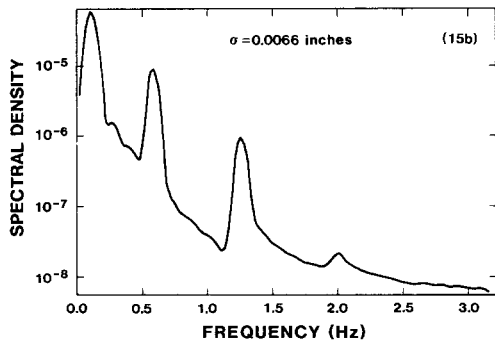


Figure 15. (a) Displacement response of center of platform in Z-direction due to wave loads only.
 (b) PSD of response.



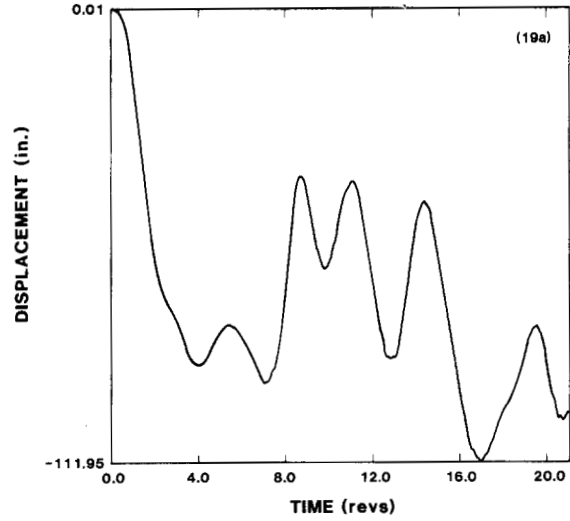
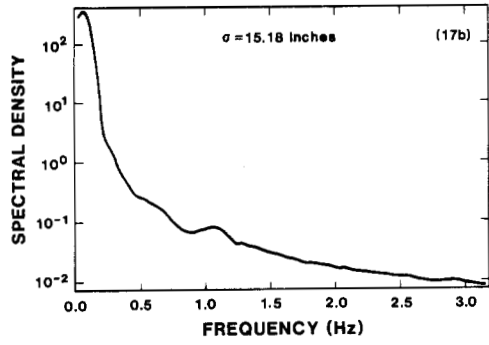


Figure 17. (a) Displacement response of top of turbine in Z-direction due to wind loads only.
(b) PSD of response.

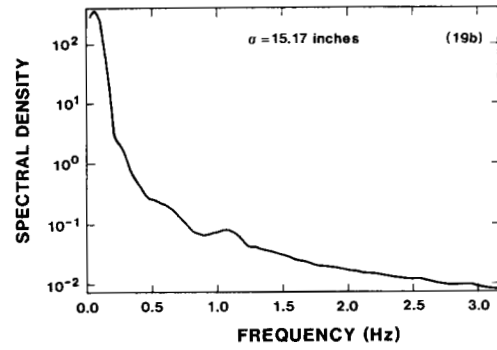
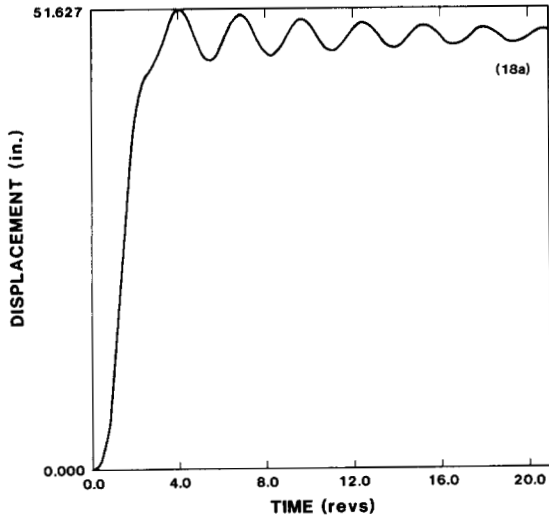


Figure 19. (a) Displacement response of top of turbine in Z-direction due to wind and wave loads.
(b) PSD of response.

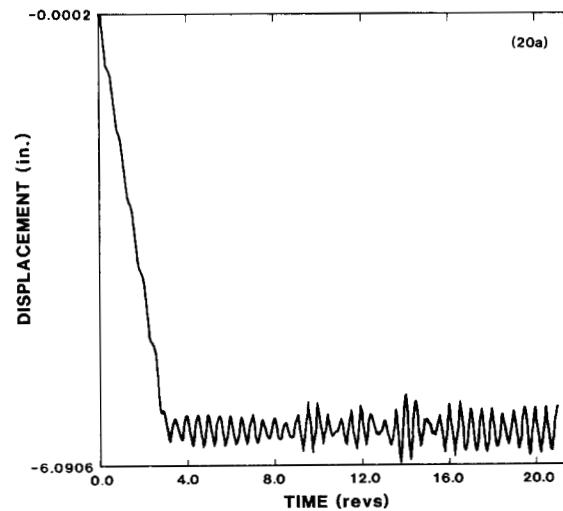
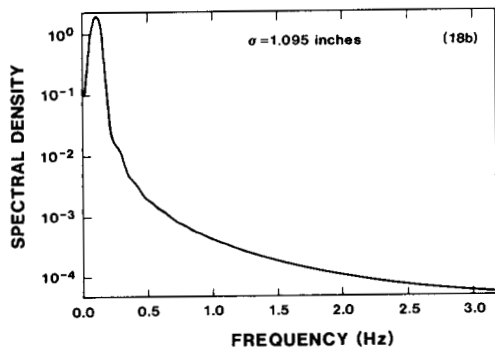


Figure 18. (a) Displacement response of top of turbine in Z-direction due to wave loads only.
(b) PSD of response.

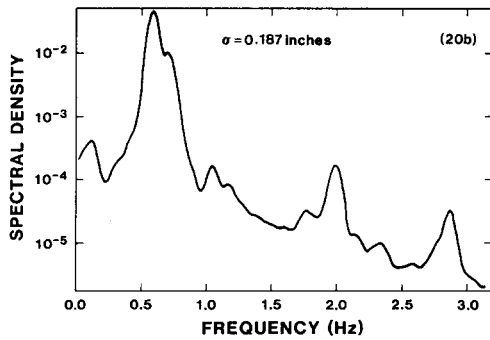


Figure 20. (a) Displacement response of center of platform in Y-direction due to wind loads only.
(b) PSD of response

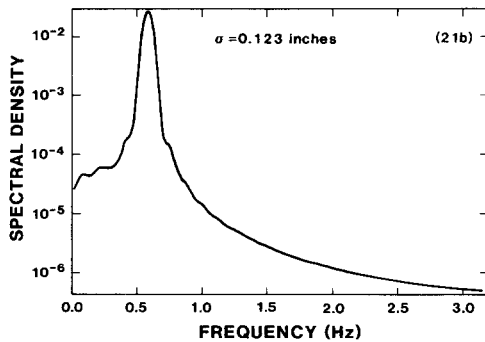
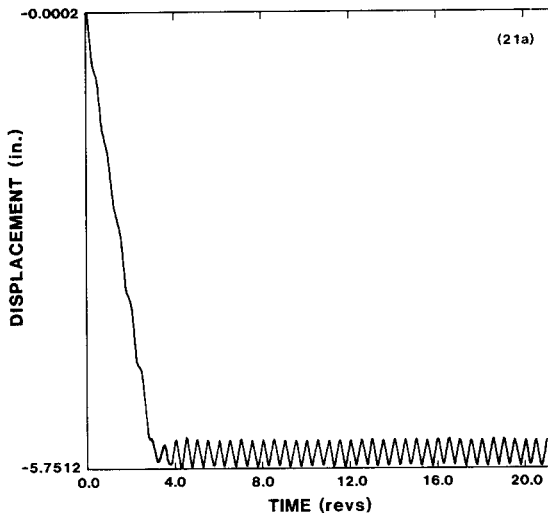
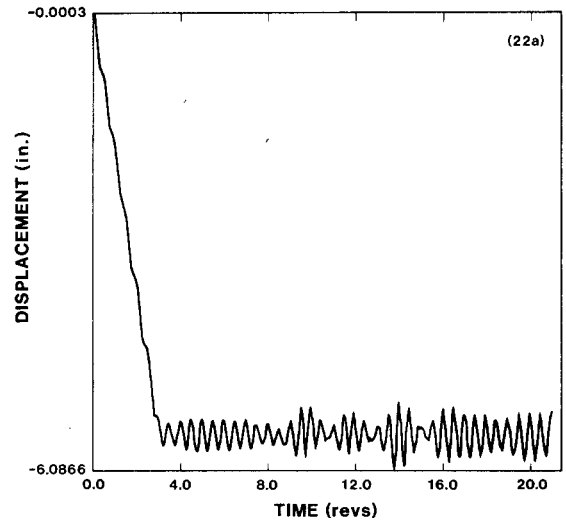


Figure 21. (a) Displacement response of center of platform in Y-direction due to wave loads only.
(b) PSD of response.

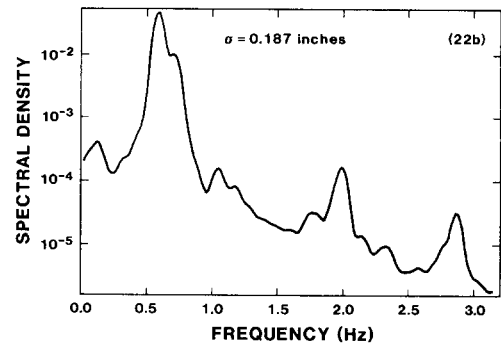


Figure 22. (a) Displacement response of center of tower in Y-direction due to wind and wave loads.
(b) PSD of response.

DISCUSSION OF RESULTS

The frequency content in the form of a PSD and the root mean square responses are useful measures of response derived from the displacement time history. The frequency content of the structural response indicates the natural modes activated by the applied loads. Mean square response can be useful to fatigue calculations. The numerical example presented in this paper is primarily a demonstration of the use of this code. The platform in the present structure is relatively stiff; therefore, wave-induced response is low. Any structure can be modeled with this computer program, and other structures would yield different results.

In all the displacement time responses shown, the wind loads are applied as a gradual linear ramped function over the first four rotor revolutions. The steady-state response is not expected until after the loads are fully applied. The Pierson-Moskowitz PSD was used as the underlying spectral content of random wave height generation given a 27-mph mean wind. The PSD of displacement response is shown for

each load case history. The PSD was generated for the steady-state response of the turbine. The initial 6.66 revolutions of response were truncated before PSD calculation. The final 14.33 revolutions of response were used in PSD calculations. The PSD was calculated by first removing up to a second-order trend from the signal, calculating the autocovariance, multiplying the autocovariance by the Parzen window, and taking the Fourier transform. The smoothing parameter, M, of the Parzen window is the highest number of lags for the autocovariance. M was chosen to be 171 for a time series of 512 points. Primary response is found in the first high peak in the low frequency range and represents static response of the structure in the frequency range of both the wind and wave loads. The time series of the response shows high frequency response superimposed on a lower frequency. The high frequency response indicates a very stiff structure. The greatest response occurs when natural frequencies of the rotating turbine fall on integral values of turbine rotation, in particular 2P (0.58 Hz), 4P (1.167 Hz), 7P (2.042 Hz), and 10P (2.917 Hz). The corner of the platform in the Z-direction behaves similarly to the center of the platform, which indicates rigid-body response in the Z-direction. The corner and center of the platform both show high frequency response due to resonances of the turbine. The top of the tower oscillates at a single low frequency. The center of the platform responds in the Y-direction primarily at the 2P excitation due to turbine rotation. The other directions of response do not represent the most significant response and are not included.

CONCLUSIONS

OFFSHORE HAWTDYN represents a unique capability to analyze the structural response of wind turbines supported on ocean platforms and is essential in designing these turbines. Computer software calculates the structural dynamic displacement response, and the PSD and mean square of response. Several numerical examples are presented to demonstrate the use of this computer code.

REFERENCES

1. Lobitz, D. W., "A NASTRAN-Based Computer Program for Structural Dynamic Analysis of Horizontal Axis Wind Turbines," European Wind Energy Conference, Commission of the European Communities, October 1984, pp. 385-393.
2. Patton, E. M., and Wilson, R. E., "Design Analysis of Performance and Aerodynamic Loading of Non-Flexible Horizontal Axis Wind Turbines," Oregon State University, RLO/2227-78-2, UC-60, August 1978.
3. Veers, P. S., "Modeling Stochastic Wind Loads on Vertical Axis Wind Turbines," Sandia National Laboratories, SAND83-1909, September 1984.
4. Frost, Walter, Long, D. H., and Turner, R. E., "Engineering Handbook on the Atmospheric Environment Guideline for Use in Wind Turbine Generator Development," NASA Technical Paper, 1359, December 1979.
5. Pierson, W. J., and Moskowitz, L., "A Proposed Spectral Form for Fully Developed Wind Seas Based on the Similarity Theory of Kitaigorodskii," Journal of Geophysical Research, Vol. 69, 1964.
6. Ochi, M. K., "Waves for Mooring System Design," Technical Note N1604, Civil Engineering Laboratory, Naval Construction Battalion Center, U.S. Navy, Port Hueneme, Calif., March 1981.
7. Wilson, J. F., ed., Dynamics of Offshore Structures, John Wiley and Sons, Inc., N.Y., 1984.

APPENDIX I

Generation of Random Time Signals While Preserving the Power Spectral Density

Any signal can be represented by a sum of harmonic components. In the case of a periodic function, a discrete, periodic Fourier series will represent it. A single period of the time signal is represented by a finite sequence of numbers that is continuously extended. A non-periodic function is represented by a continuous Fourier series (or Fourier integral). In this analysis, a continuous, non-periodic time signal is represented by a discrete, periodic Fourier series. This approximation is an accurate representation of the real signal when Δt is chosen so that the highest frequency, $1/2\Delta t$, captured in the approximation is greater than any frequency found in the original signal. Therefore a section of a non-periodic signal can be made discrete and assumed to be periodic and represented by:

$$x_j = \sum_{k=0}^{N-1} X_k e^{i2\pi kj/N - \phi_k} \quad j = 0, 1, \dots, N-1 \quad (17)$$

where,

$$X_k = \sum_{j=0}^{N-1} x_j e^{-i2\pi jk/N - \phi_k} \quad k = 0, 1, \dots, N-1. \quad (18)$$

The ϕ_k term is a uniformly distributed random variable, within the range of $-\pi$ to π , used to generate a zero-mean, weakly stationary stochastic process. The inclusion of ϕ_k in Equation 17 effectively generates a random signal by summing many harmonics with random phase. It is of particular interest to create a zero-mean, real-time signal. Certain conditions must be imposed on this representation of x_j to make the signal real-valued with zero mean. These conditions are

1. Set N = power of 2, so each generated time series will have 2^n data points
2. X_k is real-valued for $k = 1, 2, \dots, N/2-1$
3. $X_0 = X_{N/2} = 0$
4. $X_{N/2+k} = X_{N/2-k}$ for $k = 1, 2, \dots, N/2-1$
5. $\phi_k = \text{Uniform } [-\pi, \pi]$, for $k = 1, 2, \dots, N/2-1$
6. $\phi_0 = \phi_{N/2} = 0$
7. $\phi_{(N/2)+k} = -\phi_{(N/2)-k}$ for $k = 1, 2, \dots, (N/2)-1$.

Equation (17) can be rewritten to explicitly show how the signal adds around $N/2$;

$$X_{(N/2)-k} e^{i(2\pi j[(N/2)-k]/N - \phi_{(N/2)-k})} + X_{(N/2)+k} e^{i(2\pi j[(N/2)+k]/N - \phi_{(N/2)+k})}$$

Asserting conditions #4 and #7;

$$\begin{aligned} &= X_{(N/2)-k} [e^{i\pi j} e^{-i2\pi jk/N} e^{-i\phi_{(N/2)-k}} + e^{i\pi j} e^{i2\pi jk/N} e^{i\phi_{(N/2)-k}}] \\ &= X_{(N/2)-k} \cos j\pi (e^{-i[2\pi jk/N + \phi_{(N/2)-k}]} + e^{i[2\pi jk/N + \phi_{(N/2)-k}]}) \\ &= 2 X_{(N/2)-k} \cos j\pi \cos [2\pi jk/N + \phi_{(N/2)-k}] \end{aligned}$$

With the above calculation shown to be true, Equation 17 can be written as:

$$\begin{aligned} x_j &= X_0 e^{-i\phi_0} + X_{N/2} e^{-i\phi_{N/2}} e^{i\pi j} + 2 \sum_{k=1}^{(N/2)-1} X_{(N/2)-k} \cos j\pi \cos [2\pi jk/N + \phi_{(N/2)-k}] \\ &\text{for } j = 0, 1, \dots, N-1. \end{aligned}$$

Asserting condition #6;

$$\begin{aligned} x_j &= X_0 + X_{N/2} \cos j\pi + 2 \sum_{k=1}^{(N/2)-1} X_{(N/2)-k} \cos j\pi \cos [2\pi jk/N + \phi_{(N/2)-k}] \\ &\text{for } j = 0, 1, \dots, N-1. \end{aligned}$$

Asserting conditions #3 and #2;

$$\begin{aligned} x_j &= 2 \sum_{k=1}^{(N/2)-1} X_{(N/2)-k} \cos j\pi \cos [2\pi jk/N + \phi_{(N/2)-k}] \\ &\text{for } j = 0, 1, \dots, N-1. \end{aligned}$$

This is explicitly real-valued with zero-mean. This can be transformed to be expressed more compactly. It can be shown that

$$\begin{aligned} &\cos(2\pi j[(N/2)-k]/N - \phi_{(N/2)-k}) = \cos j\pi \cos [2\pi jk/N + \phi_{(N/2)-k}]. \end{aligned}$$

Starting with

$$\begin{aligned} &\cos(2\pi j[(N/2)-k]/N - \phi_{(N/2)-k}) \\ &= 1/2 \left(e^{i[2\pi j(N/2-k)/N - \phi_{N/2-k}]} + e^{-i[2\pi j[(N/2)-k]/N - \phi_{(N/2)-k}]} \right) \\ &= 1/2 [e^{i\pi j} e^{-i2\pi jk/N} e^{-i\phi_{(N/2)-k}} + e^{-i\pi j} e^{i2\pi jk/N} e^{i\phi_{(N/2)-k}}] \\ &= 1/2 \cos j\pi (e^{-i[2\pi jk/N + \phi_{(N/2)-k}]} + e^{i[2\pi jk/N + \phi_{(N/2)-k}]}) \end{aligned}$$

$$= \cos j\pi \cos[2\pi jk/N + \phi_{(N/2)-k}]$$

An intermediate form of Equation (17) is

$$x_j = 2 \sum_{k=1}^{(N/2)-1} X_{(N/2)-k} \cos(2\pi j[(N/2)-k]/N - \phi_{(N/2)-k})$$

for $j = 0, 1, \dots, N-1$.

It is possible to expand the sum to include the zero term and the $N/2$ term since they are zero;

$$x_j = 2 \sum_{k=0}^{N/2} X_{(N/2)-k} \cos(2\pi j[(N/2)-k]/N - \phi_{(N/2)-k})$$

for $j = 0, 1, \dots, N-1$.

Reversing the order of the sum;

$$x_j = 2 \sum_{k=0}^{N/2} X_k \cos(2\pi jk/N - \phi_k) \text{ for } j = 0, 1, \dots, N-1.$$

This sum explicitly produces a real-valued, zero-mean random time signal. It is possible to create a signal having a very specific underlying frequency content by determining the values of the X_k 's. This is accomplished through the use of the power spectral density. The power spectral density is the Fourier transform of the autocovariance. The discrete autocovariance is $E[x_j x_{j+q}]$. This is the "expected" or average value of the signal multiplied by itself at an incremental time, q , in advance. It is possible to use the complex conjugate of x_j in the autocovariance since x_j is a real signal, and the complex conjugate of a real number is the number itself.

$$\text{Discrete autocovariance} = E[x_j^* x_{j+q}].$$

$$= E \left[\sum_{k=0}^{N-1} X_k e^{i\phi_k} e^{-i2\pi jk/N} \sum_{m=0}^{N-1} X_m e^{-i\phi_m} e^{i2\pi(j+q)m/N} \right]$$

$$= \sum_{k=0}^{N-1} \sum_{m=0}^{N-1} X_k X_m e^{-i2\pi jk/N} e^{i2\pi(j+q)m/N} E[e^{i\phi_k} e^{-i\phi_m}]$$

$$\text{Note that } E[e^{i\phi_k} e^{-i\phi_m}] = \begin{cases} 0 & m \neq k \\ 1 & m = k \end{cases}.$$

$$\text{Therefore, } E[x_j x_{j+q}] = R_{XX}(\tau_q) = \sum_{k=0}^{N-1} X_k^2 e^{i2\pi qk/N}$$

$$S_{XX}(\omega_m) = \frac{\Delta t}{2\pi} \sum_{q=0}^{N-1} R_{XX}(\tau_q) e^{-i2\pi qm/N}$$

for $m = 0, 1, \dots, N-1$,

$$= \frac{\Delta t}{2\pi} \sum_{q=0}^{N-1} \left[\sum_{k=0}^{N-1} X_k^2 e^{i2\pi qk/N} \right] e^{-i2\pi qm/N}$$

$$= \frac{\Delta t}{2\pi} \sum_{k=0}^{N-1} X_k^2 \sum_{q=0}^{N-1} e^{i2\pi q(k-m)/N}$$

$$= \frac{N\Delta t}{2\pi} (X_m)^2.$$

$$\text{Therefore } (X_m) = [\Delta\omega S_{XX}(\omega_m)]^{1/2}.$$

The power spectral density is a symmetric function, symmetric about zero because autocovariance is real. This represents power over negative frequencies. This symmetric PSD is called a two-sided PSD, $S_{XX}(\omega)$. Sometimes the PSD is represented to have power only over positive frequencies, where the function over positive frequencies is multiplied by two which captures the total power of the two-sided PSD in the one-sided PSD. If the PSD of interest is a one-sided PSD, $G_{XX}(\omega)$, as is often available in the literature, then $X_k = [1/2 \Delta\omega G_{XX}(\omega)]$.

DISTRIBUTION:

Advanced Alternative Energy
Solutions
5673 W. Las Positas Boulevard
Suite 205
P.O. Box 5246
Pleasanton, CA
Attn: Ugur Ortobasi

Alcoa Technical Center (5)
Aluminum Company of America
Alcoa Center, PA 15069
Attn: D. K. Ai
J. T. Huang
J. R. Jombock
M. Klingensmith
J. L. Prohaska

Alternative Sources of Energy
Milaca, MN 56353
Attn: L. Stoiaken

Amarillo College
Amarillo, TX 79100
Attn: E. Gilmore

American Wind Energy Association
1017 King Street
Alexandria, VA 22314

Dr. A. S. Barker
Trinity Western
7600 Glover Road
Langley, BC
CANADA V3A 4R9

Battelle-Pacific Northwest
Laboratory
P.O. Box 999
Richland, WA 99352
Attn: L. Wendell

Bechtel Group, Inc.
P.O. Box 3965
San Francisco, CA 94119
Attn: B. Lessley

Dr. George Bergeles
Dept. of Mechanical Engineering
National Technical University
42, Patission Street
Athens, GREECE

Bonneville Power Administration
P.O. Box 3621
Portland, OR 97208
Attn: N. Butler

Burns & Roe, Inc.
800 Kinderkamack Road
Oradell, NJ 07649
Attn: G. A. Fontana

Canadian Standards Association
178 Rexdale Blvd.
Rexdale, Ontario, M9W 1R3
CANADA
Attn: T. Watson

Monique Carpentier
Energy, Mines and Resources
National Research Council
of Canada
Montreal Road
Ottawa, Ontario
CANADA K1A 0R6

Professor V. A. L. Chasteau
School of Engineering
University of Auckland
Private Bag
Auckland, NEW ZEALAND

Colorado State University
Dept. of Civil Engineering
Fort Collins, CO 80521
Attn: R. N. Meroney

Commonwealth Electric Co.
Box 368
Vineyard Haven, MA 02568
Attn: D. W. Dunham

M. M. Curvin
11169 Loop Road
Soddy Daisy, TN 37379

Department of Economic Planning
and Development
Barrett Building
Cheyenne, WY 82002
Attn: G. N. Monsson

Otto de Vries
National Aerospace Laboratory
Anthony Fokkerweg 2
Amsterdam 1017
THE NETHERLANDS

DOE/ALO
Albuquerque, NM 87115
Attn: G. P. Tennyson

DOE/ALO
Energy Technology Liaison Office
NGD
Albuquerque, NM 87115
Attn: Capt. J. L. Hanson, USAF

DOE Headquarters (20)
Wind/Oceans Technologies Division
1000 Independence Avenue
Washington, DC 20585
Attn: L. J. Rogers
P. R. Goldman

J. B. Dragt
Netherlands Energy Research
Foundation
(E.C.N.)
Physics Department
Westerduinweg 3 Petten (nh)
THE NETHERLANDS

Electric Power Research Institute
3412 Hillview Avenue
Palo Alto, CA 94304
Attn: E. Demeo
F. Goodman

Dr. Norman E. Farb
10705 Providence Drive
Villa Park, CA 92667

Alcir de Faro Orlando
Pontificia Universidade Catolica-
PUC/Rj
Mechanical Engineering Department
R. Marques de S. Vicente 225
Rio de Janeiro, BRAZIL

Fayette Manufacturing Corporation
P.O. Box 1149
Tracy, CA 95378-1149
Attn: W. Thompson

FloWind Corporation (2)
1183 Quarry Lane
Pleasanton, CA 94566
Attn: L. Schienbein
B. Im

A. D. Garrad
Garrad Hasson
10 Northampton Square
London EC1M 5PA
UNITED KINGDOM

H. Gerardin
Mechanical Engineering Department
Faculty of Sciences and Engineering
Universite Laval-Quebec, G1K 7P4
CANADA

Dr. I. J. Graham
Southern University
Department of Mechanical Engineering
P.O. Box 9445
Baton Rouge, LA 70813-9445

R. T. Griffiths
University College of Swansea
Dept. of Mechanical Engineering
Singleton Park
Swansea, SA2 8PP
UNITED KINGDOM

Helion, Inc.
Box 445
Brownsville, CA 95919
Attn: J. Park, President

Indal Technologies, Inc. (2)
3570 Hawkestone Road
Mississauga, Ontario
CANADA L5C 2V8
Attn: D. Malcolm
C. Wood

Institut de Recherche d'Hydro-Quebec
1800, Montee Ste-Julie
Varenes, Quebec, JOL 2P.O.
CANADA
Attn: Bernard Masse

Iowa State University
Agricultural Engineering, Room 213
Ames, IA 50010
Attn: L. H. Soderholm

K. Jackson
West Wind Industries
P.O. Box 1705
Davis, CA 95617

M. Jackson
McAllester Financial
1816 Summit
W. Lafayette, IN 47906

Kaiser Aluminum and Chemical
Sales, Inc.
14200 Cottage Grove Avenue
Dolton, IL 60419
Attn: A. A. Hagman

Kaiser Aluminum and Chemical
Sales, Inc.
6177 Sunol Blvd.
P.O. Box 877
Pleasanton, CA 94566
Attn: D. D. Doerr

Kansas State University
Electrical Engineering Department
Manhattan, KS 66506
Attn: Dr. G. L. Johnson

R. E. Kelland
The College of Trades and Technology
P.O. Box 1693
Prince Philip Drive
St. John's, Newfoundland, A1C 5P7
CANADA

Kinetics Group, Inc.
P.O. Box 1071
Mercer Island, WA 98040
Attn: J. Sladky, Jr.

KW Control Systems, Inc.
RD#4, Box 914C
South Plank Road
Middletown, NY 10940
Attn: R. H. Klein

L. K. Liljergren
1260 S.E. Walnut #5
Tustin, CA 92680

L. Liljidadhl
Building 005, Room 304
Barc-West
Beltsville, MD 20705

Olle Ljungstrom
FFA, The Aeronautical Research
Institute
Box 11021
S-16111 Bromma, SWEDEN

Robert Lynette
R. Lynette & Assoc., Inc.
15042 NE 40th Street
Suite 206
Redmond, WA 98052

Massachusetts Institute of
Technology
77 Massachusetts Avenue
Cambridge, MA 02139
Attn: Professor N. D. Ham
W. L. Harris, Aero/Astro
Dept.

H. S. Matsuda
Composite Materials Laboratory
Pioneering R&D Laboratories
Toray Industries, Inc.
Sonoyama, Otsu, Shiga, JAPAN 520

G. M. McNerney
US Wind Power
160 Wheeler Road
Burlington, MA 01803

Michigan State University
Division of Engineering Research
East Lansing, MI 48825
Attn: O. Krauss

Napier College of Commerce and
Technology
Tutor Librarian, Technology Faculty
Colinton Road
Edinburgh, EH10 5DT
ENGLAND

National Rural Electric
Cooperative Assn
1800 Massachusetts Avenue, NW
Washington, DC 20036
Attn: Wilson Prichett, III

Natural Power, Inc.
New Boston, NH 03070
Attn: Leander Nichols

New Mexico Engineering
Research Institute
Campus P.O. Box 25
Albuquerque, NM 87131
Attn: G. G. Leigh

Ohio State University
Aeronautical and Astronautical Dept.
2070 Neil Avenue
Columbus, OH 43210
Attn: Professor G. Gregorek

Oklahoma State University
Mechanical Engineering Dept.
Stillwater, OK 76074
Attn: D. K. McLaughlin

Oregon State University
Mechanical Engineering Dept.
Corvallis, OR 97331
Attn: R. E. Wilson

Pacific Gas & Electric Co.
3400 Crow Canyon Road
San Ramon, CA 94583
Attn: T. Hillesland

Ion Paraschivoiu
Department of Mechanical Engineering
Ecole Polytechnique
CP 6079
Succursale A
Montreal H3C 3A7
CANADA

Jacques Plante
Hydro Quebec
Place Dupuis Ile etage
855 est rue Ste-Catherine
Montreal, Quebec
CANADA H2L 4P5

J. M. Turner Technologies, Inc.
P.O. Box 1058
Schenectady, NY 12301-1058
Attn: Eric N. Hinrichsen

Public Service Co. of New Hampshire
1000 Elm Street
Manchester, NH 03105
Attn: D. L. C. Frederick

Public Service Company of New Mexico
P.O. Box 2267
Albuquerque, NM 87103
Attn: M. Lechner

RANN, Inc.
260 Sheridan Ave., Suite 414
Palo Alto, CA 94306
Attn: A. J. Eggers, Jr.

Dr. R. Ganesh Rajagopalan,
Asst. Prof.
Aerospace Engineering Department
Iowa State University
404 Town Engineering Bldg.
Ames, IA 50011

The Resources Agency
Department of Water Resources
Energy Division
P.O. Box 388
Sacramento, CA 95802
Attn: R. G. Ferreira

Reynolds Metals Company
Mill Products Division
6601 West Broad Street
Richmond, VA 23261
Attn: G. E. Lennox

R. G. Richards
Atlantic Wind Test Site
P.O. Box 189
Tignish P.E.I., COB 2B0
CANADA

Riso National Laboratory
Postbox 49
DK-4000 Roskilde
DENMARK
Attn: Troels Friis Pedersen
Helge Petersen

Dr. Ing. Hans Ruscheweyh
Institut für Leichbau
Technische Hochschule Aachen
Wullnerstrasse 7
FEDERAL REPUBLIC OF GERMANY

Beatrice de Saint Louvent
Etablissement d'Etudes et de
Recherches
Météorologiques
77 Rue de Servès
92106 Boulogne-Billancourt Cedex
FRANCE

Gwen Schreiner
Librarian
National Atomic Museum
Albuquerque, NM 87185

Arnan Seginer
Professor of Aerodynamics
Technion-Israel Institute of
Technology
Aeronautical Engineering Dept.
Haifa
ISRAEL

Mr. Farrell Smith Seiler, Editor
Wind Energy News Service
P.O. Box 4008
St. Johnsbury, VT 05819

David Sharpe
Dept. of Aeronautical Engineering
Queen Mary College
Mile End Road
London, E1 4NS
UNITED KINGDOM

Kent Smith
Instituto Tecnológico Costa Rica
Apartado 159 Cartago
COSTA RICA

Solar Energy Research Institute
1617 Cole Boulevard
Golden, CO 80401
Attn: R. W. Thresher

Bent Sorenson
Roskilde University Center
Energy Group, Bldg. 17.2
IMFUFA
P.O. Box 260
DK-400 Roskilde
DENMARK

Peter South
ADECON
32 Rivalda Road
Weston, Ontario, M9M 2M3
CANADA

Southern California Edison
Research & Development Dept., Room
497
P.O. Box 800
Rosemead, CA 91770
Attn: R. L. Scheffler

G. Stacey
The University of Reading
Department of Engineering
Whiteknights, Reading, RG6 2AY
ENGLAND

Stanford University
Dept. of Aeronautics and
Astronautics Mechanical Engineering
Stanford, CA 94305
Attn: Holt Ashley

Dr. Derek Taylor
Alternative Energy Group
Walton Hall
Open University
Milton Keynes, MK7 6AA
UNITED KINGDOM

R. J. Templin (3)
Low Speed Aerodynamics Laboratory
NRC-National Aeronautical
Establishment
Montreal Road
Ottawa, Ontario, K1A 0R6
CANADA

Texas Tech University (2)
Mechanical Engineering Dept.
P.O. Box 4289
Lubbock, TX 79409
Attn: J. W. Oler

K. J. Touryan
Moriah Research
6200 Plateau Dr.
Englewood, CO 80111

Tulane University
Dept. of Mechanical Engineering
New Orleans, LA 70018
Attn: R. G. Watts

United Engineers and Constructors,
Inc.
P.O. Box 8223
Philadelphia, PA 19101
Attn: A. J. Karalis

Universal Data Systems
5000 Bradford Drive
Huntsville, AL 35805
Attn: C. W. Dodd

University of California
Institute of Geophysics
and Planetary Physics
Riverside, CA 92521
Attn: Dr. P. J. Baum

University of Colorado
Dept. of Aerospace Engineering
Sciences
Boulder, CO 80309
Attn: J. D. Fock, Jr.

University of Massachusetts
Mechanical and Aerospace
Engineering Dept.
Amherst, MA 01003
Attn: Dr. D. E. Cromack

University of Oklahoma
Aero Engineering Department
Norman, OK 73069
Attn: K. Bergey

University of Sherbrooke
Faculty of Applied Science
Sherbrooke, Quebec, J1K 2R1
CANADA
Attn: A. Laneville
P. Vittecoq

The University of Tennessee
Dept. of Electrical Engineering
Knoxville, TN 37916
Attn: T. W. Reddoch

USDA, Agricultural Research Service
Southwest Great Plains Research
Center
Bushland, TX 79012
Attn: Dr. R. N. Clark

W. A. Vachon
W. A. Vachon & Associates
P.O. Box 149
Manchester, MA 01944

Dirk Vandenberghe
State Univ. of Ghent
St. Pietersnieuwstraat 41
9000 Ghent
BELGIUM

Washington and Lee University
P.O. Box 735
Lexington, VA 24450
Attn: Dr. R. E. Akins

Washington State University
Dept. of Electrical Engineering
Pullman, WA 99163
Attn: F. K. Bechtel

West Texas State University
Government Depository Library
Number 613
Canyon, TX 79015

West Texas State University
Department of Physics
P.O. Box 248
Canyon, TX 79016
Attn: V. Nelson

West Virginia University
Dept. of Aero Engineering
1062 Kountz Avenue
Morgantown, WV 26505
Attn: R. Walters

D. Westlind
Central Lincoln People's Utility
District
2129 North Coast Highway
Newport, OR 97365-1795

Wichita State University
Aero Engineering Department (2)
Wichita, KS 67208
Attn: M. Snyder
W. Wentz

Wind Power Digest
P.O. Box 700
Bascom, OH 44809
Attn: Michael Evans

Wisconsin Division of State Energy
8th Floor
101 South Webster Street
Madison, WI 53702
Attn: Wind Program Manager

1520 C. W. Peterson
1522 R. C. Reuter, Jr.
1523 J. H. Biffle
1524 A. K. Miller
1524 D. W. Lobitz
1550 R. C. Maydew
1552 J. H. Strickland
1556 G. F. Homicz
2525 R. P. Clark
3141 S. A. Landenberger (5)
3151 W. L. Garner (3)
3154-3 C. H. Dalin (28)
For DOE/OSTI (Unlimited
Release)
3160 J. E. Mitchell (15)
3161 P. S. Wilson
6000 D. L. Hartley
6200 V. L. Dugan
6220 D. G. Schueler
6225 H. M. Dodd (50)
6225 T. D. Ashwill
6225 D. E. Berg
6225 T. C. Bryant
6225 L. R. Gallo
6225 P. C. Klimas (30)
6225 S. D. Nicolaysen
6225 D. S. Oscar (75)
6225 M. E. Ralph
6225 D. C. Reda
6225 M. A. Rumsey
6225 L. L. Schluter

6225 W. A. Stephenson
6225 H. J. Sutherland
7542 T. L. Paez (50)
7544 D. R. Schafer
7544 J. Lauffer
8024 P. W. Dean (5)
9100 R. G. Clem
9122 T. M. Leonard
6220 A. V. Poore